The Effect of a Well-Resolved Stratosphere on Surface Climate: Differences between CMIP5 Simulations with High and Low Top Versions of the Met Office Climate Model

S. C. HARDIMAN, N. BUTCHART, AND T. J. HINTON

Met Office Hadley Centre, Exeter, Devon, United Kingdom

S. M. OSPREY AND L. J. GRAY

National Centre for Atmospheric Science, University of Oxford, Oxford, United Kingdom

(Manuscript received 25 August 2011, in final form 27 April 2012)

ABSTRACT

The importance of using a general circulation model that includes a well-resolved stratosphere for climate simulations, and particularly the influence this has on surface climate, is investigated. High top model simulations are run with the Met Office Unified Model for the Coupled Model Intercomparison Project Phase 5 (CMIP5). These simulations are compared to equivalent simulations run using a low top model differing only in vertical extent and vertical resolution above 15 km. The period 1960–2002 is analyzed and compared to observations and the European Centre for Medium-Range Weather Forecasts (ECMWF) reanalysis dataset. Long-term climatology, variability, and trends in surface temperature and sea ice, along with the variability of the annular mode index, are found to be insensitive to the addition of a well-resolved stratosphere. The inclusion of a well-resolved stratosphere, however, does improve the impact of atmospheric teleconnections on surface climate, in particular the response to El Niño–Southern Oscillation, the quasi-biennial oscillation, and midwinter stratospheric sudden warmings (i.e., zonal mean wind reversals in the middle stratosphere). Thus, including a well-represented stratosphere could improve climate simulation on intraseasonal to interannual time scales.

1. Introduction

The importance of including a well-resolved stratosphere in coupled climate models to correctly simulate aspects of surface climate has now been considered by several studies (Huebener et al. 2007; Sigmond et al. 2008; Cagnazzo and Manzini 2009; Sassi et al. 2010). These studies compare the surface fields in climate models that have a well-resolved stratosphere (so called ''high top'' models) and those with a lower top boundary and a fairly coarse vertical resolution in the stratosphere (''low top'' models). There is now general agreement that including a well-resolved stratosphere leads to better extratropical stratospheric variability, and consequently to improvements in simulated tropospheric dynamical fields. However, uncertainty remains as to which differences between high and low top models are the important ones. Sigmond et al. (2008) suggest that the differences in the climate change response between the high and low top model simulations in their study arise primarily due to differences in the settings for the parameterization schemes (and in particular orographic gravity wave drag) rather than to raising the model lid height. However, Shaw and Perlwitz (2010) suggest that the high and low top control simulations in this study differ because of wave reflection from the lid of the low top model. Sassi et al. (2010) also suggest that wave reflection from the lid in low top models leads to changes in, and a less realistic simulation of the zonal circulation and surface pressure, and that the more realistic physics included in high top models is not relevant to the changes they see.

In the present work, the high top model simulations run at the Met Office Hadley Centre for inclusion in the Coupled Model Intercomparison Project Phase 5 (CMIP5; http://cmip-pcmdi.llnl.gov/cmip5) are compared against

Corresponding author address: Steven Hardiman, Met Office, FitzRoy Road, Exeter, Devon EX1 3PB, United Kingdom.
E-mail: steven.hardiman@metoffice.gov.uk

DOI: 10.1175/JCLI-D-11-00579.1

those of a low top model that differs *only* in vertical extent and vertical resolution above 15 km (~115 hPa). All included physics, and physical parameters, are the same in both high and low top models allowing for a clean comparison of the models. The influence of including a well-resolved stratosphere on surface temperature, the annular mode indices, and atmospheric teleconnections is considered. It is demonstrated that El Niño teleconnections, the effects of the quasi-biennial oscillation (QBO) of tropical stratospheric winds, and the effects of midwinter warmings of the stratospheric polar vortex on Northern Hemisphere surface climate are not captured by the low top model.

The CMIP5 database is eventually expected to contain data from around 11 high top climate models. While this is many more than have been used for previous Intergovernmental Panel on Climate Change (IPCC) reports (e.g., CMIP3; Solomon et al. 2007)—around 11 of 32 models in CMIP5 as opposed to around 5 of 25 models in CMIP3—the majority of simulations included are still run with low top models. The aim of this study is to demonstrate that while the low top model used here can simulate realistic basic climate, and even realistic interannual variability, it is unable to capture certain aspects of stratosphere–troposphere coupling, which significantly influences surface climate.

2. Climate model and experimental setup

The climate version of the Met Office's Unified Model, the Hadley Centre Global Environmental Model (HadGEM), is available in many different configurations. The configurations used here, named HadGEM2-carbon cycle (HadGEM2-CC) (low top) and HadGEM2-carbon cycle stratosphere (HadGEM2-CCS) (high top, same as HadGEM2-CC except for the stratospheric extension), are as described in Martin et al. (2011) and initialized to run historical CMIP5 simulations as detailed in Jones et al. (2011). The horizontal resolution is 1.875° longitude × 1.25° latitude. The model includes a coupled ocean [i.e., the Hadley Centre Ocean Carbon Cycle model (HadOCC), with horizontal resolution 1° × 1° increasing in the tropics to 0.3°, 40 vertical levels, and a lower boundary at 5.3 km] and coupled carbon cycle, but no explicit interactive chemistry apart from methane oxidation. In particular, methane and ozone concentrations are prescribed (see section 4.2 of Jones et al. 2011). A detailed description of the stratospheric behavior in an earlier version of this model is given in Hardiman et al. (2010) and Osprey et al. (2010).

To allow a clean comparison, the high and low top models differ only in vertical resolution above 15 km and model lid height. The high top model has 60 vertical levels and upper boundary at 84 km. The low top model has 38 vertical levels and upper boundary at 39 km. Both model versions include a momentum-conserving nonorographic gravity wave drag parameterization (Warner and McIntyre 1999; Scaife et al. 2002), and production of stratospheric water vapor by methane oxidation (Untch and Simmons 1999; Simmons et al. 1999). Unsaturated orographic gravity waves are neglected above 40 km in both high and low top models.

The historical simulations run from 1860 to 2005. In the present study, a single realization over the whole time period, and two further ensemble members from 1960 to 2005 are run with both high and low top models. The ensemble members are branched from the main simulation by using the atmospheric and oceanic model states on 11 and 21 December 1959 from the main simulation to initialize the ensemble member simulations from 1 December 1959.

Observation and reanalysis datasets

The global 40-yr European Centre for Medium-Range Weather Forecasts (ECMWF) Re-Analysis (ERA-40; Uppala et al. 2005), a three-dimensional global reanalysis spanning the period 1960–2002 and assimilating many good-quality observations, is used as the core validation dataset in this study. As such, the period 1960–2002 is analyzed in detail in this paper. When looking at trends in sea surface temperature, mean sea level pressure, and sea ice, the Hadley Centre SST dataset (HadSST; Rayner et al. 2003) and Hadley Centre SLP dataset (HadSLP; Allan and Ansell 2006) are also used since there are concerns about ERA-40 trends in the presatellite era. These show, for the most part, agreement with ERA-40. In some cases (e.g., trends in MSLP) they demonstrate where there are uncertainties in the datasets.

For looking at the North Atlantic Oscillation (NAO), a much longer dataset is required, and years 1856–2002 from the Climatic Research Unit (CRU) dataset (http://www.cru.uea.ac.uk/cru/data/nao/) are used. Similarly a longer dataset is required when looking at El Niño teleconnections, and years 1850–2004 from the HadSLP dataset are used.

3. Surface climate

a. Climatology

Figure 1 shows the climatological annual mean surface temperature, averaged from 1960 to 2002. In general the model agrees well with the reanalysis data, capturing the highest mean temperature around 120°E in the tropics, and the low temperatures over Greenland

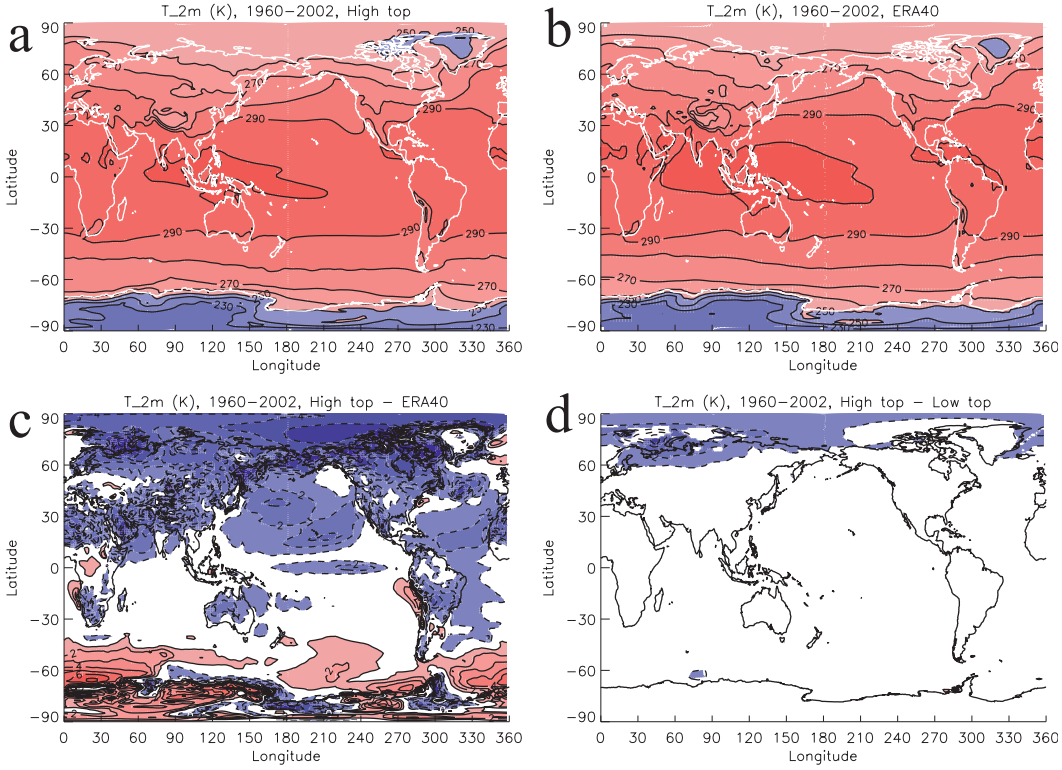

FIG. 1. Climatological annual mean surface temperature (K) averaged from 1960 to 2002: (a) high top model, (b) ERA-40, (c) high top model–ERA-40, and (d) high top model–low top model. Blue (red) shading in (c) and (d) represents cold (warm) biases in 1° graduations. In (c) and (d), only regions where the differences plotted are greater than 1 K and statistically significant at the 95% level are shaded.

and Antarctica (Figs. 1a,b). The model temperature is around 1 K lower than the ERA-40 reanalysis for the global mean and around 3 K lower over the Arctic (Fig. 1c). Figure 1c also shows a mean warm bias of 1.6 K over the Southern Ocean, which peaks at 6.7 K near 30°E. There is less than 1-K difference in the climatological surface temperature between the high top and low top models except in the northern extratropics, where the high top model is as much as 5 K lower around 45°E (Fig. 1d). When averaged over the extended Northern Hemisphere (NH) winter (November–March) rather than the whole year, this difference becomes ~9 K and can be seen in the mean sea level pressure (MSLP) field too (not shown).

b. *Variability*

As with the climatological mean temperature, the spatial structure of the interannual standard deviation of surface temperature is well captured by both high and low top versions of the model, showing local maxima in the Niño-3 region (5°S–5°N, 210°–270°E) and also in the extratropics (Fig. 2). Variability in the models differs over the eastern Pacific, with the low top model showing almost double the variability seen in the reanalysis west of South America around 15°S. The high top model shows a better-defined Niño-3 region. Both models show too much variability in the Arctic. The contrast of greater interannual variability in the surface temperature over the land than over the ocean is captured by the models, though not as strongly as is seen in the reanalysis. The interannual variability over Amazonia is far lower in the models than in the reanalysis. In the following sections the main focus is on the extratropics and El Niño, shown here to be the regions of greatest variability in surface temperature.

c. *Trends*

Figure 3 shows the trend in sea surface temperature (SST) from 1960 to 2000. Trends from the Hadley Centre SST dataset (HadSST; Rayner et al. 2003) do not provide global coverage, but they demonstrate that the trends in ERA-40 (2-m temperature) are fairly realistic (not surprising as the SSTs used as boundary conditions in the production of ERA-40 are taken from a combination of HadSST and the National Oceanic and Atmospheric Administration/National Centers for Environmental

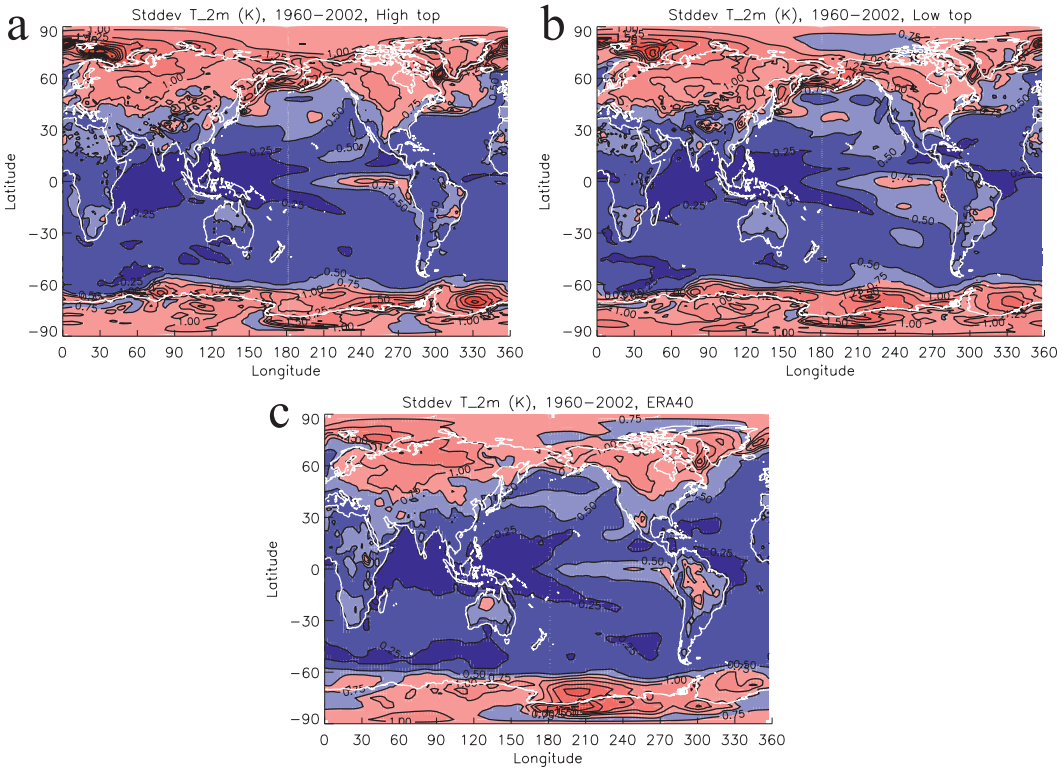

FIG. 2. Interannual standard deviation in detrended annual mean surface temperature (K), 1960–2002: (a) high top model, (b) low top model, and (c) ERA-40.

Prediction dataset; Uppala et al. 2005). Comparing ERA-40 trends to the model trends shows that neither model captures the negative trend in the polar North Atlantic, although both models show a cooling in the region of the Gulf Stream (further discussion on the North Atlantic Oscillation follows in section 4a), possibly due to the large internal variability seen in these regions (Atlantic multidecadal variability; see, e.g., Park and Latif 2008). However, the high top model trends in the northern Pacific and in the Southern Hemisphere are more realistic than those from the low top model. Slight differences between the models and reanalysis in the trend in the North Pacific may be due to the phase of the Pacific decadal oscillation (Mantua and Hare 2002; Schneider and Cornuelle 2005). The Pacific decadal oscillation in sea surface temperatures is internally generated and therefore the phase of this oscillation in the models is not expected to match that in the observations. The mean trend in global surface temperature of 0.5 K over the 40 years is well reproduced by both models.

Arctic sea ice extent is well simulated in the models (Fig. 4a) with a steady 12×10^6 km^2 annual mean extent seen up to 1970 and then a decrease of around 1.5×10^6 km^2 from 1970 to 2005. The lower polar temperatures in the high top model (Fig. 1d) lead to around 1×10^6 km^2 more Arctic sea ice in this model from 1975 onward. The mean sea ice extent in the Antarctic is severely underestimated (Fig. 4b) with around 7.5×10^6 km^2 simulated as opposed to the 10×10^6 km^2 seen in the analyses. This bias is partly attributed to the warm bias in surface temperatures over the Southern Ocean, seen in Fig. 1c. Cloud biases partially account for these warm temperatures. It is also likely that excessive heat advected from the Southern Ocean into the sea ice region at 100-m depth causes a breakdown of the thermocline and consequently affects sea ice formation. This is most pronounced in the South Atlantic sector from 0° to 50°E (J. Ridley 2011, personal communication). The models correctly simulate no trend in Antarctic sea ice extent (Fig. 4b).

4. Mean sea level pressure trends

a. Northern Hemisphere

Figure 5 shows the trend in December–January–February (DJF) MSLP in the northern extratropics from 1960 to 2002. The negative trend over the pole, surrounded by a positive trend, seen in the ERA-40 reanalysis data and HadSLP (Allan and Ansell 2006)

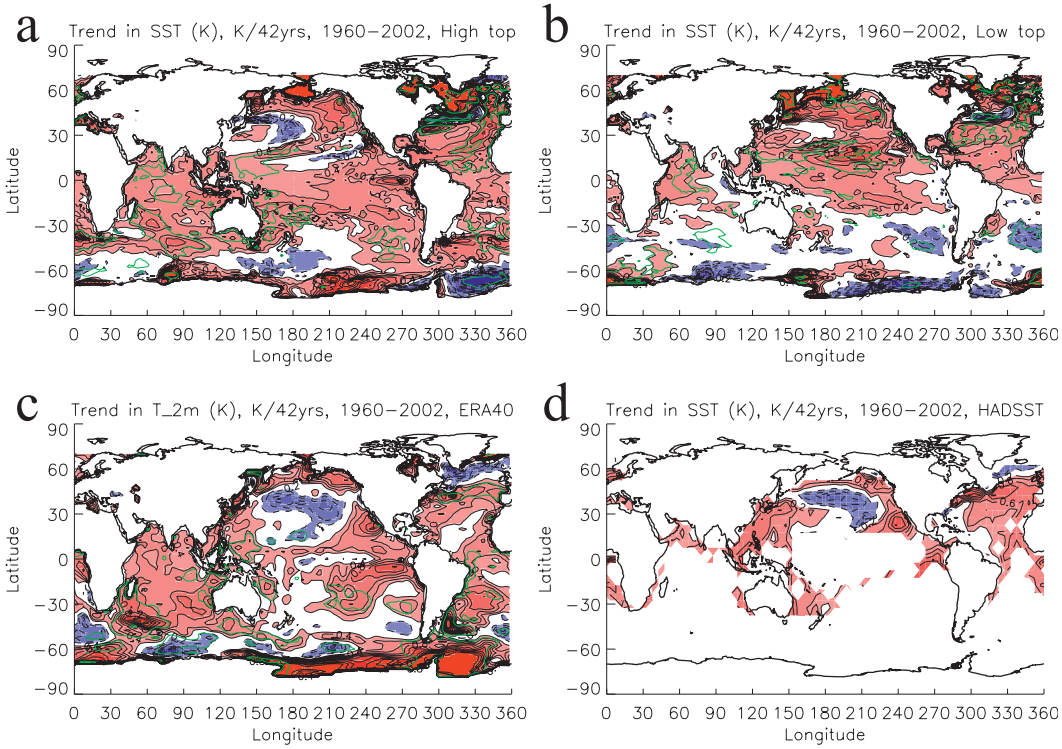

FIG. 3. Trend in SST 1960–2002 [K (42 yr)$^{-1}$] for (a) high top model, (b) low top model, (c) ERA-40, and (d) HadSST. Contour interval is 0.2 K (42 yr)$^{-1}$. Trends greater than 0.2 K (42 yr)$^{-1}$ in magnitude are shaded. Solid (dashed) contours represent positive (negative) values and the zero contour is not plotted. Green contours show regions where the trend is statistically significant at the 95% level (a)–(c).

is consistent with an increasing northern annular mode (NAM)/North Atlantic Oscillation (NAO) index (Osborn and Jones 2000; Scaife et al. 2005). HadSLP, created using marine observations taken from 2228 stations around the globe, suggests that the trend in ERA-40 is too strong, although the spatial pattern of the ERA-40 trend is accurate. The models do not reproduce this trend. The low top model shows a trend that is too weak over the Arctic and the high top model shows a trend of the wrong sign. This is clear also from Fig. 6, which shows a time series of the NAO index [calculated from MSLP(Azores) − MSLP(Iceland), and now shown for December–March (DJFM) as in Wallace 2000]. The observed strong trend from 1965

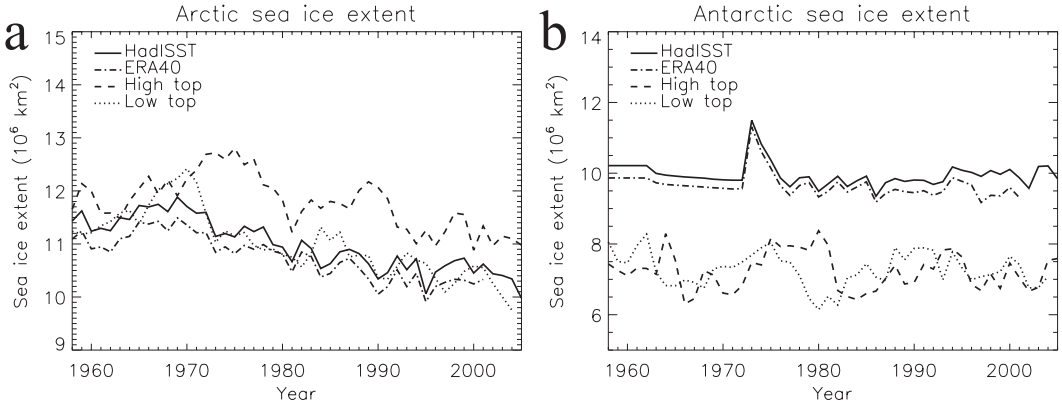

FIG. 4. Sea ice extent (10^6 km^2) in the (a) Arctic (NH) and (b) Antarctic (SH) for HadISST analyses (Rayner et al. 2003), ERA-40, high top, and low top models. The HadISST data prior to 1979 (i.e., the satellite period) in the Antarctic includes whaling fleet data but these are so sparse that the analyses are largely climatology there.

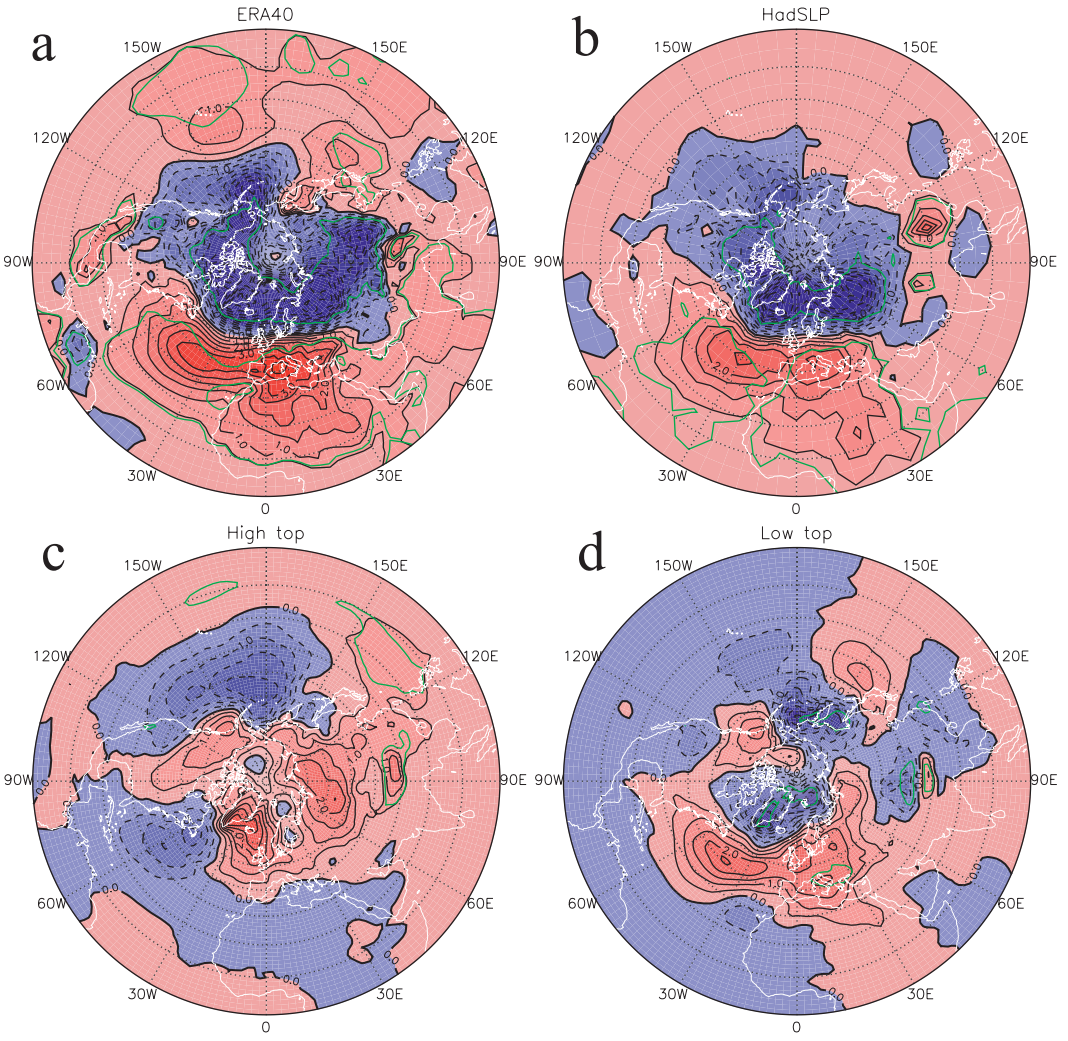

FIG. 5. Trend in MSLP [hPa (30 yr)$^{-1}$] for DJF (1960–2002) over the northern extratropics: (a) ERA-40, (b) HadSLP, (c) high top model, and (d) low top model. Solid (dashed) contours represent positive (negative) values. Contour interval is 0.5 hPa (30 yr)$^{-1}$. Green contours show regions where the trend is statistically significant at the 95% level.

to 1995 (e.g., Scaife et al. 2005) is not captured by the models. However, the magnitude of interannual variability in the NAO index is fairly accurately simulated by the models (interannual standard deviations for the detrended time series from 1960 to 2002 are 7.6 hPa for ERA-40, 6.0 hPa for the high top model, and 6.0 hPa for the low top model). Low-frequency variability in the NAO index has been linked to changes in the stratospheric zonal mean zonal wind, U, (Wallace 2000; Scaife et al. 2005) and also to changes in the ocean circulation (Hoerling et al. 2004). As such, the NAO index is likely to exhibit the internal decadal variability seen in the stratosphere (Butchart et al. 2000) and the oceans. Thus, the models may not be expected to simulate large trends in the NAO index over the same time interval (1965–95) as they are observed. This has relevance for the understanding of Fig. 5, too—were trends of the observed NAO index computed up to present day (i.e., beyond the end of the ERA-40 dataset) then Fig. 5 may look very different.

A more important question is whether the models are capable of simulating so strong a trend in the NAO index over any 30-yr time period. Figure 7 shows the distribution of 30-yr trends in the NAO index calculated from years 1856–2002 of the CRU dataset and all years (1861–2005) of the high and low top simulations. The models accurately capture the distribution of trends, and although no simulated trend is as high as the observed 12 hPa (30 yr)$^{-1}$ in 1965–95, trends of 10 hPa (30 yr)$^{-1}$ are simulated. A best-fit Gaussian curve is shown for

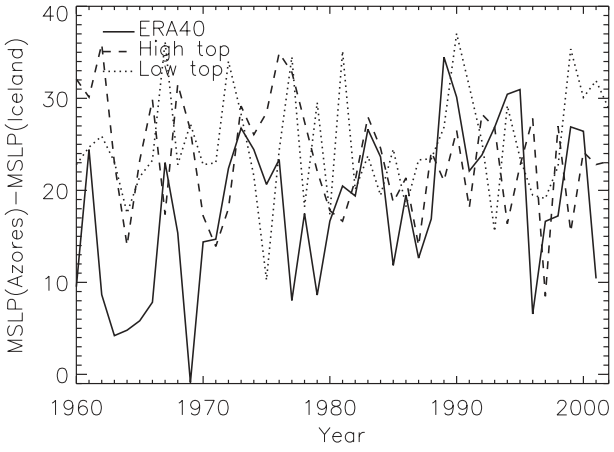

FIG. 6. NAO index for DJFM, calculated from MSLP(Azores) − MSLP(Iceland) (hPa).

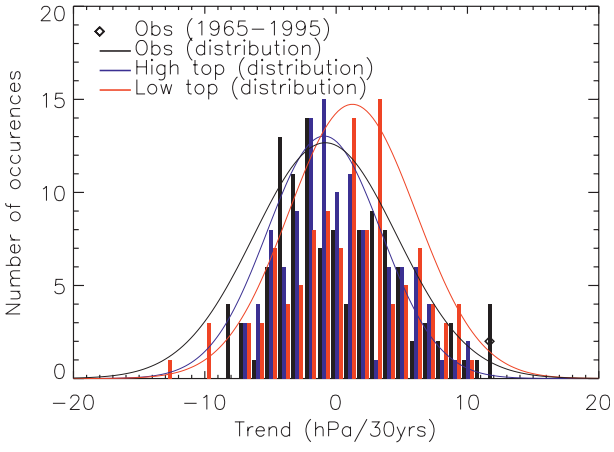

FIG. 7. The distribution of 30-yr running trends in the DJFM NAO index, based on years 1861–2005 in the model simulations and 1856–2002 in the CRU dataset (http://www.cru.uea.ac.uk/cru/data/nao/). The trends are calculated from 118 (116) data points from 147 (145) yr of data for the observations(models). Best-fit Gaussian curves are added for each histogram. (No claims are made about statistical independence of the data points in these histograms—indeed, the four observed 12-hPa trends are for 30-yr periods starting in 1962, 1963, 1965, and 1966.)

each distribution. The mean values of the Gaussian (−0.83 in the observations) represent a small long-term drift in the NAO index. However, these drifts are not significant, and indeed are also found in the 240-yr high and low top preindustrial control simulations (+0.02 in the high top and +0.35 in the low top simulation). The histograms in Fig. 7 are not found to be significantly different from each other. In summary, Fig. 7 suggests that the decadal trends in the NAO index as simulated by the models are not inconsistent to those observed in the real atmosphere.

b. Southern Hemisphere

The corresponding trends in DJF MSLP from 1960 to 2002 in the southern extratropics are shown in Fig. 8 (e.g., Arblaster and Meehl 2006). These trends have been strongly linked to the external forcing from ozone depletion leading to a stronger Southern Hemisphere polar night jet, which in turn leads to an increase in the southern annular mode (SAM) index and increased zonal wind over the Southern Ocean in DJF (Son et al. 2010; Le Quéré et al. 2007; Lenton et al. 2009). Since this trend is in part externally forced, Fig. 8 shows the mean of the three ensemble member trends, for both high and low top models. Again, the negative trend over the pole, surrounded by a positive trend, is consistent with an increasing SAM index. As in the Northern Hemisphere, ERA-40 appears to overestimate the magnitude of the trend compared to HadSLP [note that ERA-40 trends in presatellite years (i.e., prior to 1979) in the Southern Hemisphere are not reliable]. Both models simulate the correct trend but substantially underestimate its magnitude, compared with the ERA-40 reanalysis.

As in Son et al. (2010), Fig. 9a demonstrates that the associated trend in the zonal mean zonal wind, U, from 1960 to 2000 in ERA-40 is statistically significant throughout the troposphere and lower stratosphere. However, the simulated ensemble mean trend in both high and low top models (Figs. 9c,g) is weak and not statistically significant. This lack of significance is partly due to the large interannual variability in U found in the models (standard deviation up to 4 m s^{-1} as opposed to up to 3 m s^{-1} in ERA-40) and partly due to the weak trend, which is consistent with a weak negative meridional gradient in the tropospheric temperature trend from 45° to 65°S in the lower troposphere (Figs. 9b,d,h). The weak (though still significant) trend in U in the stratosphere around 60°S is due to the ozone-induced cooling in the model at around 200 hPa in the polar region, but is far weaker than that evident in ERA-40 (Fig. 9b) and also in measurements from Antarctic radiosonde stations (Thompson and Solomon 2002). A slight positive trend in U is simulated around 80°S where a negative trend is found in the reanalysis. This is due to a tropospheric cooling in the model, compared to warming there in the reanalysis (as is also evident in Fig. 3). Also, note that the modeled trends are slightly too far equatorward, especially so in the low top model (Figs. 9a,c,g). As in Son et al. (2010), who find no statistically significant difference between the zonal mean zonal wind trends in ensembles of high and low top models, here the trends in the high and low top models are very similar, probably because both models use the same prescribed ozone fields.

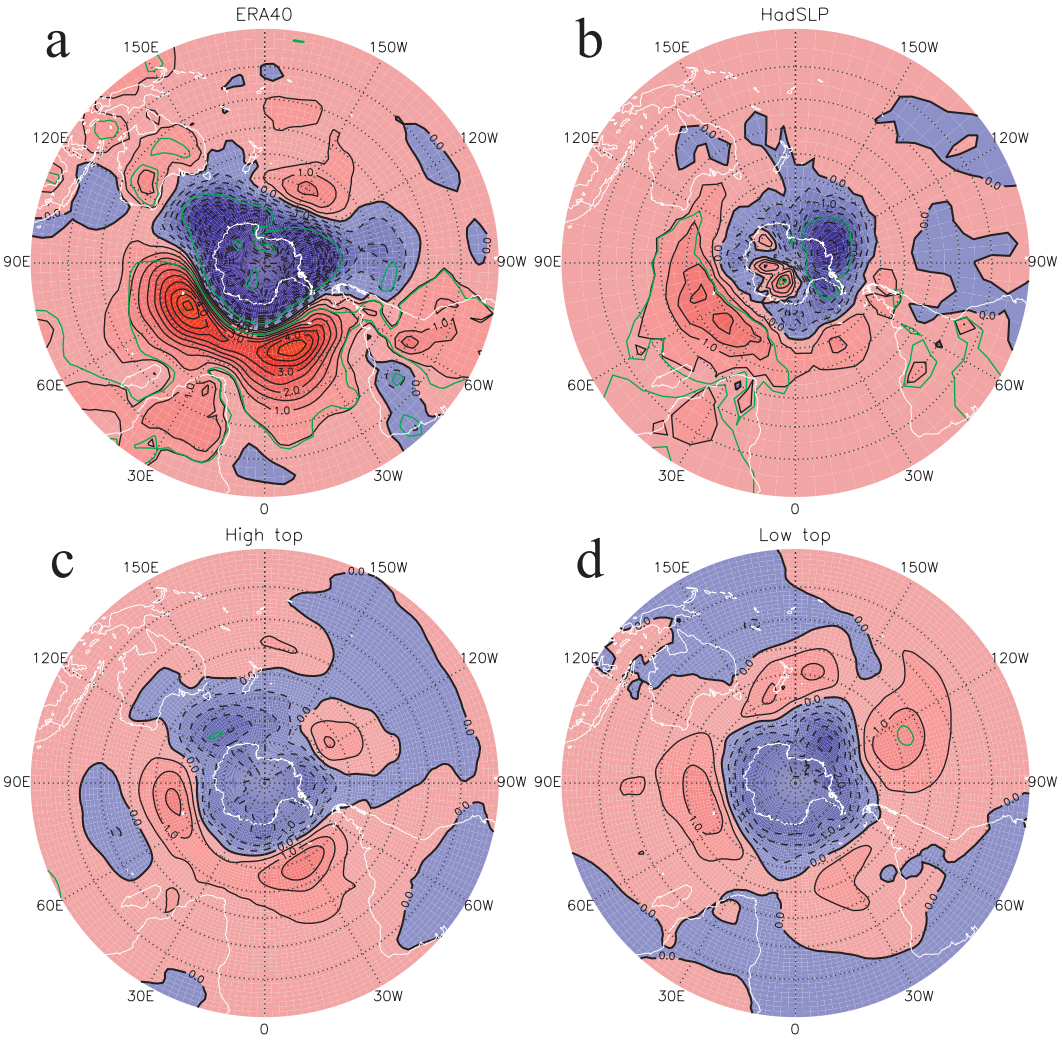

FIG. 8. Trend in MSLP [hPa (30 yr)$^{-1}$] for DJF, 1960–2002, over the southern extratropics: (a) ERA-40, (b) HadSLP, (c) high top model (ensemble mean trend), and (d) low top model (ensemble mean trend). Solid (dashed) contours represent positive (negative) values. Contour interval is 0.5 hPa (30 yr)$^{-1}$. Green contours show regions where the trend is statistically significant at the 95% level.

To further investigate this, a three member ensemble identical to the high top model ensemble, but run with constant 1960s ozone concentrations, is computed and shows a very similar ensemble mean trend in *U* (Fig. 9e). The stratospheric temperature trend in the constant ozone ensemble is, as expected, very different to that in the high top historical simulations (Fig. 9f), and therefore because of thermal–wind relations the vertical gradient in *U* is not the same in the stratosphere as in the historical simulations, nor is it as significant. However, more midlatitude warming in the troposphere (around 50°S and 400 hPa) occurs in these constant ozone simulations, slightly strengthening the tropospheric *U* trend. Overall, the constant ozone simulations suggest that the trend in zonal mean zonal wind in all these simulations has little to do with ozone depletion.

A significant trend in *U* throughout the troposphere *is* found in an ensemble of simulations run for CMIP5 with an equivalent low top model that includes interactive tropospheric chemistry, though stratospheric ozone is still prescribed (not shown; simulations described in Jones et al. 2011). Interactive chemistry may be an advantage since any gradients in the tropospheric chemical fields may then follow gradients in the dynamical fields, strengthening the resulting signals such as increasing zonal mean zonal wind over the Southern Ocean. However, it is recognized that these results do not explicitly prove the need for interactive chemistry to capture this signal. Indeed, Son et al. (2010) show that most models

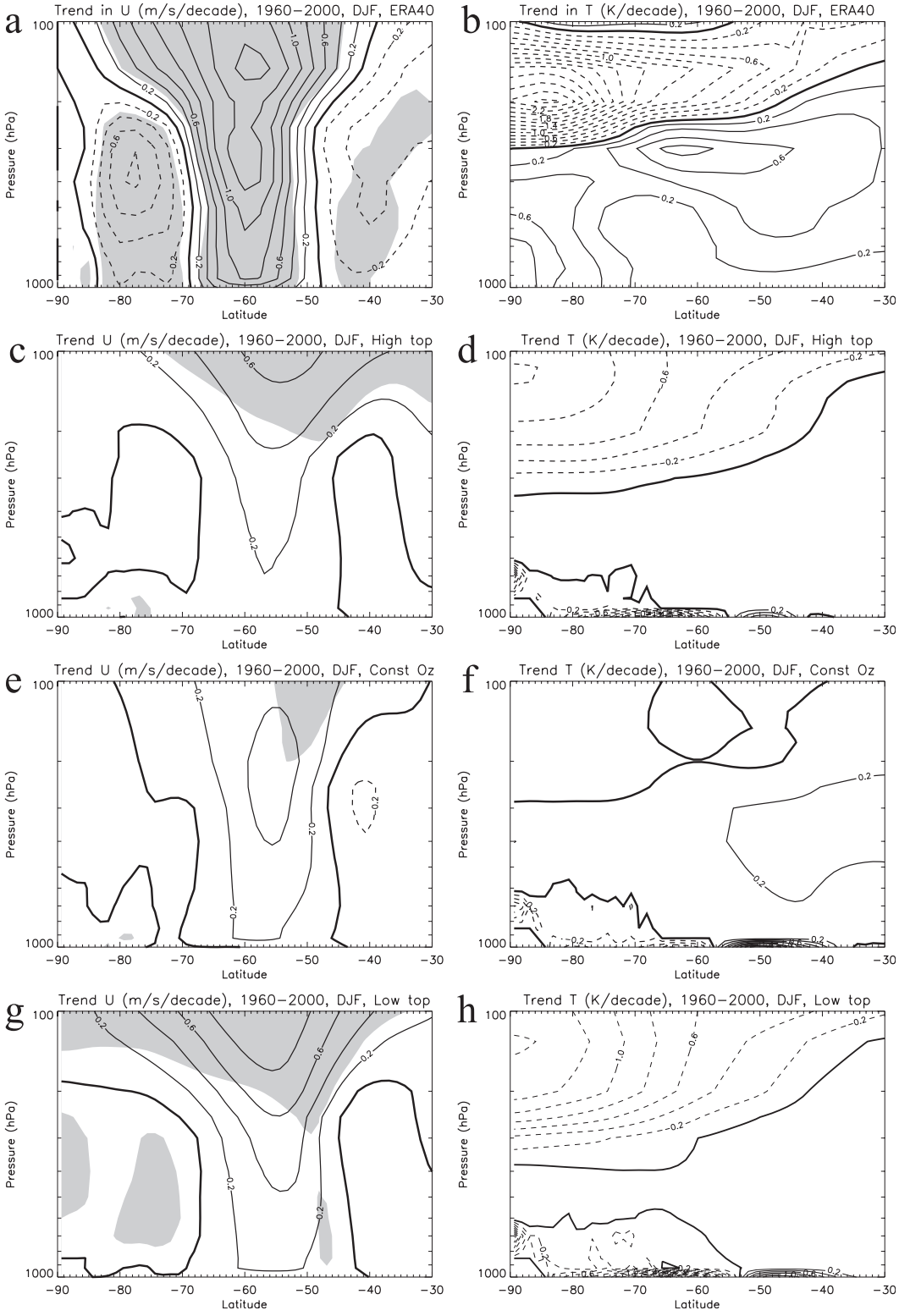

FIG. 9. Trend in zonal mean zonal wind U (m s^{-1} decade^{-1}), and temperature T (K decade^{-1}) in DJF from 1960 to 2000 for (a),(b) ERA-40; (c),(d) high top model; (e),(f) high top model with constant 1960 ozone; and (g),(h) low top model. Note that ERA-40 trends in presatellite years (prior to 1979) in the Southern Hemisphere are not reliable. Solid (dashed) contours represent positive (negative) trends. Shading in U panels represents significance at the 95% confidence level. T trends are significant at the 95% confidence level almost everywhere, so for clarity shading is not included in these panels. Model ensemble mean trends are shown.

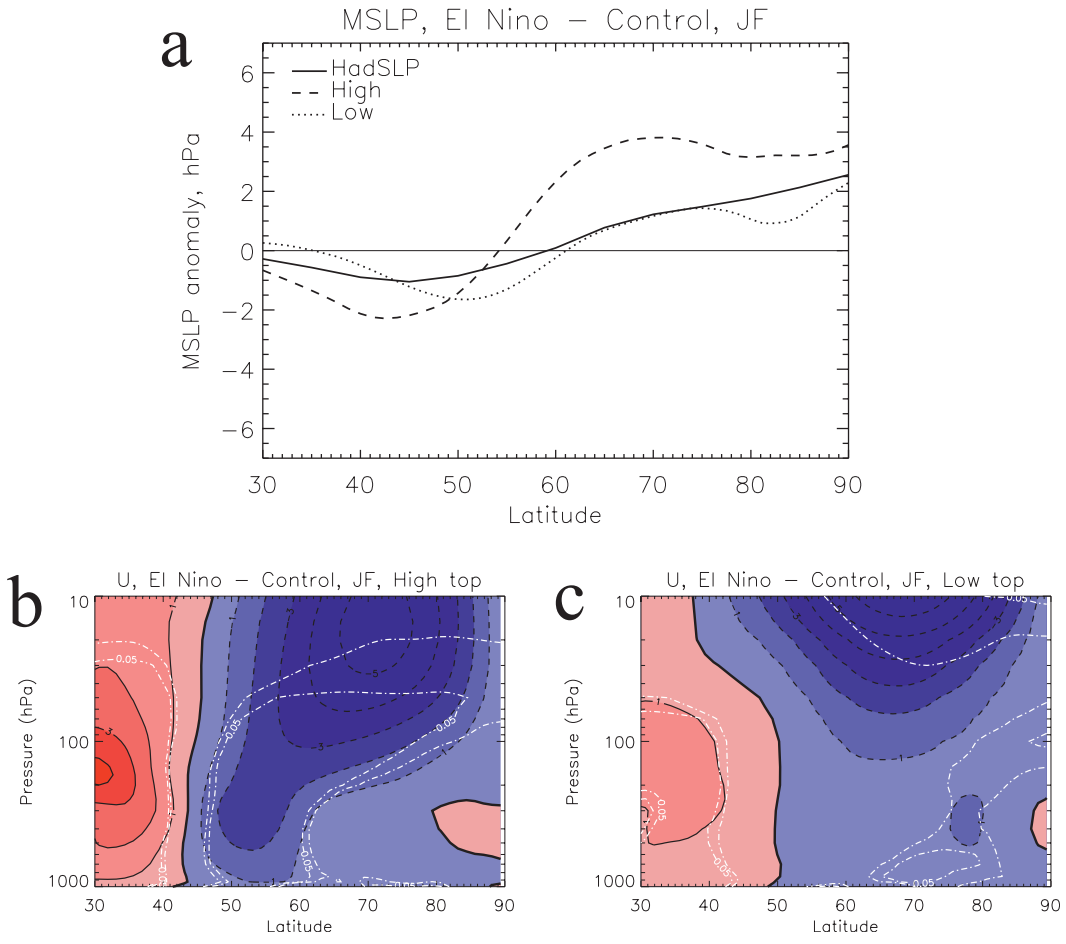

FIG. 10. (a) Difference in composites of MSLP over El Niño years (years in which the Niño-3 index is greater than one standard deviation above the mean) and control years (years in which the absolute magnitude of the Niño-3 index is less than one-third standard deviation from the mean), averaged from 30°W–30°E. Corresponding composites of zonal mean zonal wind for (b) high top and (c) low top models. Model years 1960–2005 from all ensemble members are used (a total of 135 years for each model), and years 1850–2004 from HadSLP. The Niño-3 index is calculated from sea surface temperature anomalies in the region 5°S–5°N, 210°–270°E. White dot–dashed lines show statistical significance at the 90% and 95% levels, respectively.

with either interactive stratospheric chemistry or prescribed ozone do capture the observed trend.

In summary, the sign of the trend in the zonal mean zonal wind over the Southern Ocean from 1960 to 2000 is captured in these simulations, although the trend is severely underestimated and not statistically significant. Contrary to previous studies, the trend does not appear to be due to ozone depletion in this model.

5. Teleconnections

The previous two sections considered long-term climate variability and trends, and showed little difference between high and low top versions of the model. The effects of specific stratospheric processes on surface climate on year-to-year time scales are now considered.

a. El Niño

One such effect is the well-known teleconnection of the El Niño–Southern Oscillation (ENSO) with MSLP in the northern extratropics in winter. In El Niño years anomalously high MSLP is found in northern high latitudes and anomalously low MSLP is found in the northern midlatitudes, projecting onto a negative NAO pattern (van Loon and Madden 1981). Bell et al. (2009, see their Fig. 7) demonstrated, using an idealized general circulation model, that a model with a degraded stratosphere was not able to capture this teleconnection, whereas a model with a well-resolved stratosphere could (see also Cagnazzo and Manzini 2009). Figure 10a of the current paper shows that in the Met Office Unified Model the signal of anomalously positive MSLP in the

northern high latitudes and anomalously low MSLP in midlatitudes in January–February in El Niño years is captured in both the high top and the low top models. However, the amplitude of this signal (i.e., the difference in high-latitude MSLP and midlatitude MSLP) is about double in the high top model (6 hPa) than that seen in the low top model (3 hPa). Although HadSLP seems to agree more with the low top model, HadSLP is known to underestimate the interannual variability in MSLP (see section 3.5 of Rayner et al. 2003).

The stratospheric pathway for this teleconnection is via the stratospheric polar vortex. El Niño years lead to a weaker stratospheric polar vortex (Braesicke and Pyle 2004; Manzini et al. 2006; Ineson and Scaife 2009), which in turn influences MSLP (Baldwin and Dunkerton 1999; Perlwitz and Harnik 2004). Although the low top model does simulate a stratospheric polar vortex, the signal of a weaker vortex in El Niño years is small in the lower stratosphere and appears confined to the stratosphere in the low top model, whereas this signal is larger throughout the stratosphere and extends to the surface in the high top model (Figs. 10b,c).

While there is uncertainty in the strength of the ENSO teleconnection in observations, the model simulations suggest that the stratosphere strengthens this connection between the tropics and high latitudes.

b. QBO

The QBO of the tropical zonal mean zonal wind is internally generated in the high top model (Scaife et al. 2000; Bushell et al. 2010). The low top model also includes the nonorographic gravity wave drag scheme, which contributes to the generation of this QBO, but still does not simulate a QBO. Given the limited differences between the high and low top models, this is likely due to coarser vertical resolution in the lower to midstratosphere in the low top model. However, the absence of the semi-annual oscillation and the lower model lid in the low top model may also play a role. The QBO can directly influence surface climate, as demonstrated by Garfinkel and Hartmann (2011), who show that the meridional circulation induced by the QBO extends downward into the troposphere and interacts with subtropical eddies such that the zonal wind and temperature anomalies associated with the induced circulation extend farther downward to the surface. The zonal wind anomalies form a ''horseshoe'' shape in the height–latitude plane, as can be seen in Fig. 11. The pattern of the anomalies seen in ERA-40 (Figs. 11a,c) is well captured in the high top model in both Pacific and Atlantic sectors (Figs. 11b,d), with significant anomalies extending to the surface. The slight difference between the reanalysis and model anomalies at around 50°N and 100 hPa in the Pacific sector is not significant and the sign of the anomaly in this region is sensitive to the years included in the composite, as is the case in the region around 30°N and 100 hPa in the Atlantic sector. The composites in Fig. 11 are suggestive of correlations between equatorial zonal winds at around 50 hPa and zonal winds at other latitudes and altitudes. Both high and low top models simulate these correlations. However, in the low top model there is very little variability in the equatorial zonal winds at 50 hPa, and these correlations will not relate to variability on the time scale of the QBO. Thus there will be no predictability in surface climate due to the phase of the QBO in the low top model.

Associated with these zonal wind anomalies are significant anomalies in MSLP, shown in Figs. 11e,f [these anomalies are similar to the QBO-induced anomalies found in geopotential height at 50 hPa by Marshall and Scaife (2009)]. Because of geostrophic balance, these MSLP anomalies are a maximum at the latitudes where the zonal wind anomalies are zero at the surface. The anomalous low in MSLP over the Pacific and anomalous high in the Atlantic seen in the reanalysis are well captured by the model, though the position of the anomalous high over the Atlantic is farther equatorward in the model and poleward of 50°N the anomalies have different signs.

By not simulating a QBO, the low top model fails to include an important aspect of tropical variability in the stratosphere or any direct effects of the QBO on the surface climate.

c. Sudden warmings

A further way in which the stratosphere can influence surface climate is via midwinter stratospheric sudden warmings (SSWs) of the polar vortex (e.g., Charlton and Polvani 2007). The widely used World Meteorological Organization (WMO) definition of SSWs (easterly zonal mean winds at 10 hPa and 60°N) is used here—zonal mean wind reversal prevents planetary wave propagation and so represents a dynamical change in the state of the stratosphere. The frequency of these SSWs throughout Northern Hemisphere winter is well simulated by the high top model, whereas the low top model simulates very few SSWs (about 1 every 5 years on average as opposed to approximately 1 every 2 years observed, not shown). Figure 12a shows that the climatological stratospheric jet strength in Northern Hemisphere winter is too strong in the low top model, especially in February and March. While the variability in the low top model is realistic, the extreme easterly events (i.e., SSWs), are not sufficiently frequent or sufficiently strong. Further, the extreme westerly events (cold winters) are

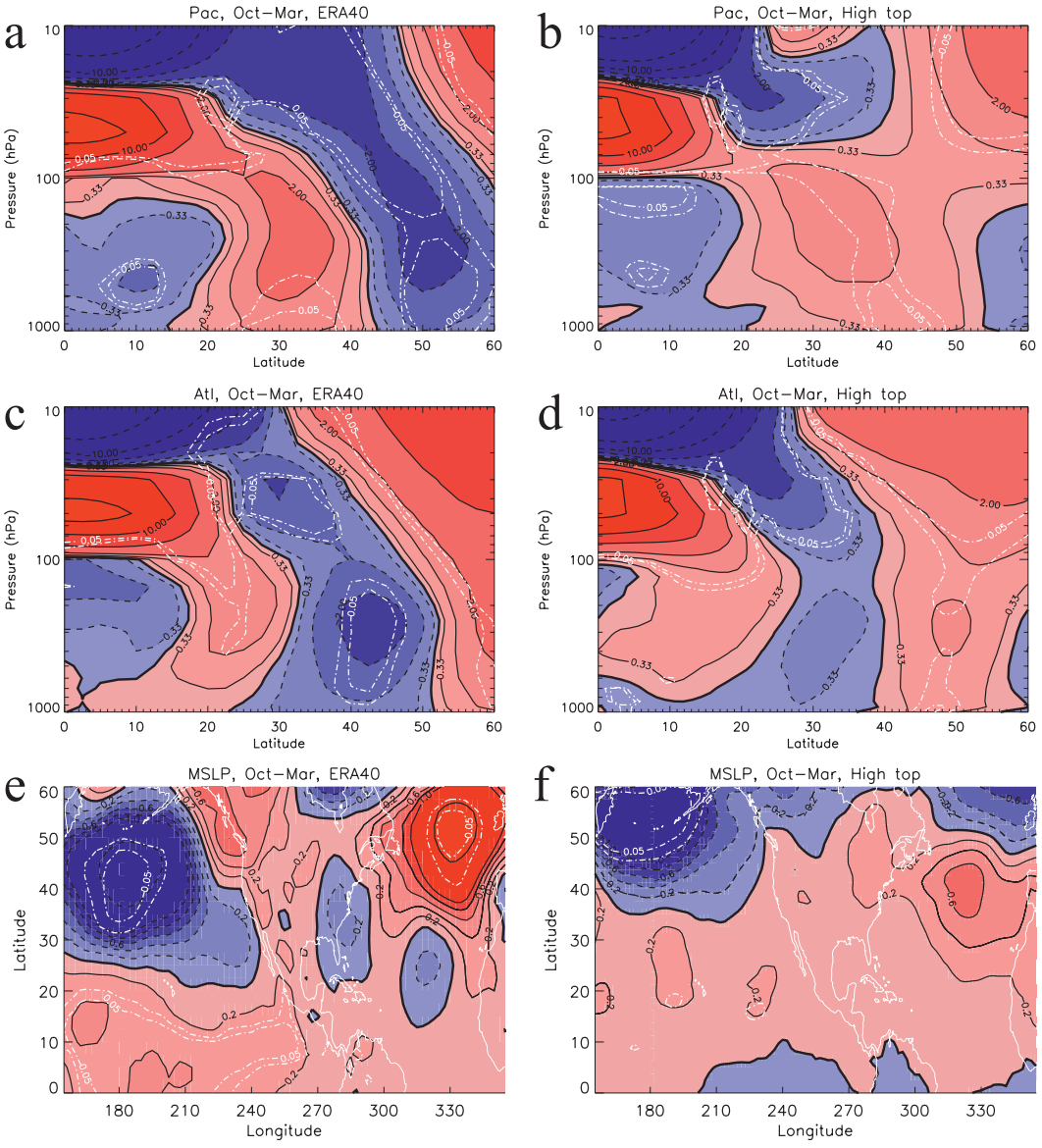

FIG. 11. Zonal mean zonal wind, composited over QBO east–QBO west years, using high top model years from 1860 to 2005 and ERA-40 from 1960–2002 in NH extended winter (October–March) for (a),(b) Pacific (160°–200°E) and (c),(d) Atlantic (310°–350°E) sectors. Corresponding anomalies in MSLP for (e) ERA-40 and (f) high top model. White dot–dashed lines show statistical significance at the 90% and 95% levels, respectively.

too strong (see also Martin et al. 2011). Throughout the period 1960–2005, no SSWs are simulated by the low top model during Northern Hemisphere winter until mid-February. The range in the jet strength (shown also in Fig. 12a) is realistic in the low top model, but the mean value of the jet strength is too strong.

In the month following a SSW, a response is found in MSLP and surface temperature (Scaife and Knight 2008; Kolstad et al. 2010; Marshall and Scaife 2010). Figure 12b shows the mean MSLP response averaged over the month following an SSW for all SSWs from 1958–2002 in ERA-40. Anomalously high pressure over the pole and low pressure in the extratropics indicates an anomalously negative NAM. Figure 12c shows the corresponding anomalous surface temperature. This impact on surface MSLP and temperature is simulated by the high top model. Figures 12d,e show anomalous MSLP and surface temperature, respectively, averaged over the month following an SSW for all SSWs from 1960–2005 in the high top model simulation. The response is broadly the same as that found in ERA-40, albeit

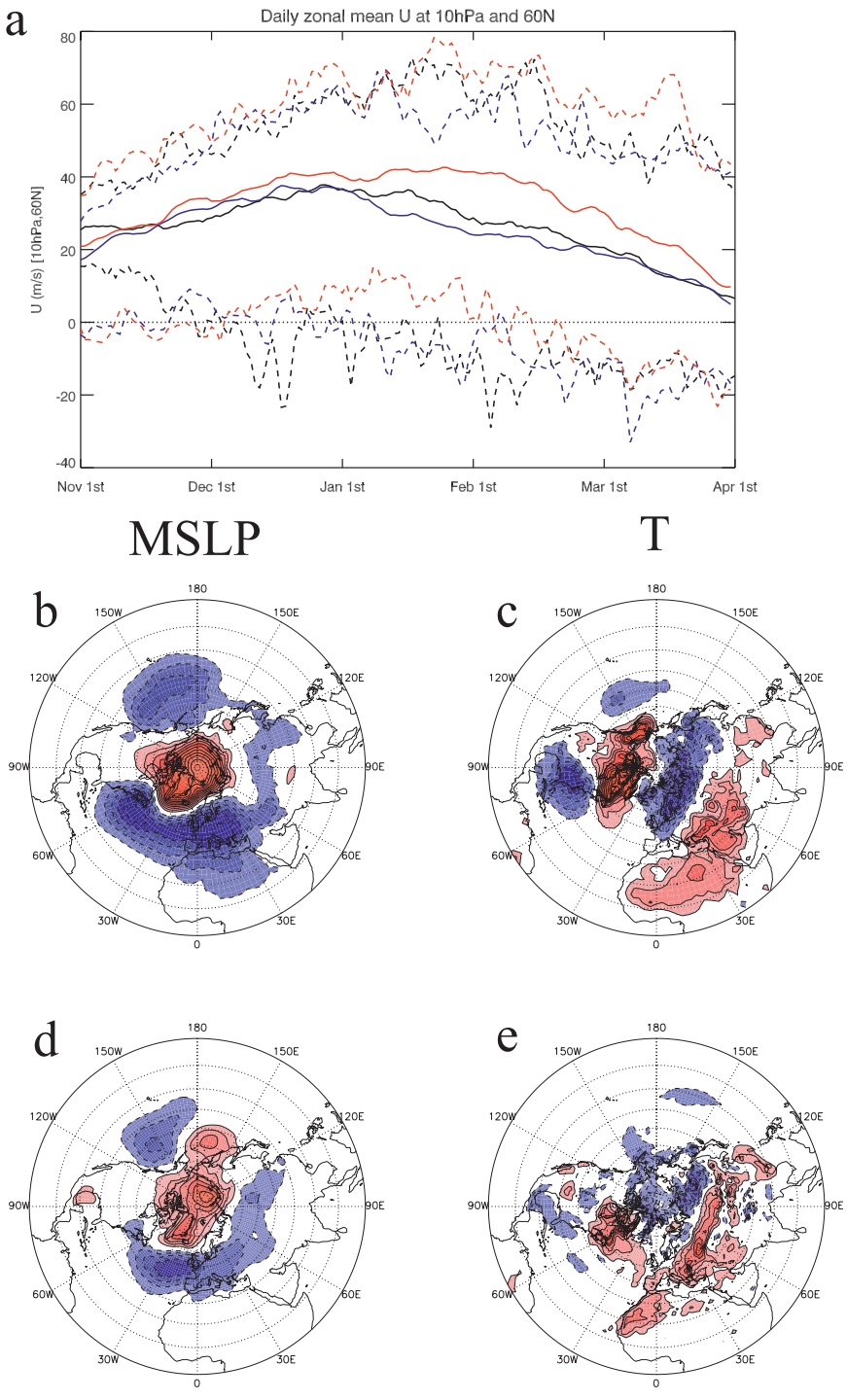

FIG. 12. (a) Zonal mean zonal wind at 10 hPa and 60°N, for ERA-40 (1958–2002, black), high top model (1960–2005, blue), and low top model (1960–2005, red). Solid lines show climatological mean values and dashed lines show full range of values for each day. (b) Mean of the MSLP anomalies averaged over the month following an SSW for all SSWs from 1958–2002 in ERA-40. Contour interval is 0.5 hPa and zero contour is not plotted. (c) As in (b), but for surface temperature. Contour interval is 0.25 K and zero contour is not plotted. (d) Mean of the MSLP anomalies averaged over the month following an SSW for all SSWs from 1960–2005 in the high top model simulation. Contours as in (b). (e) As in (d), but for surface temperature. Contours as in (c). Solid (dashed) contours represent positive (negative) values in (b)–(e).

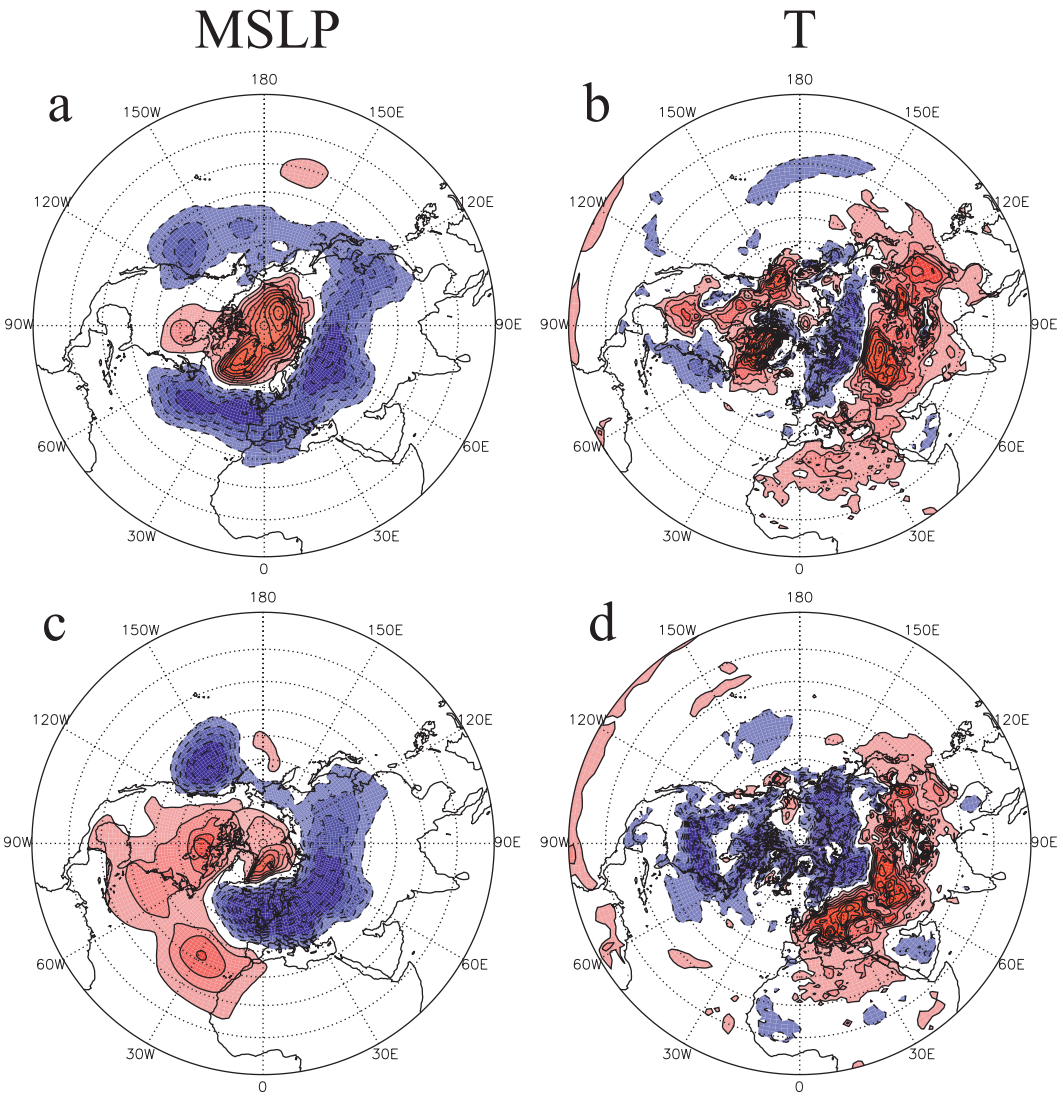

FIG. 13. The mean response in (a),(c) MSLP and (b),(d) surface temperature averaged over the months following events in which U (60°N, 10 hPa) is less than two standard deviations below its mean value (November–March), for the high top model in (a) and (b) and low top model in (c) and (d). Contour intervals and line styles are as in Figs. 12b–e.

with localized differences in the surface temperature response.

Because of the absence of SSWs, the low top model will miss this important effect. However, the variability in the strength of the stratospheric polar vortex (shown in Fig. 12a to be realistic in the low top model also) will still have an impact on MSLP and surface temperature. Figure 13 shows the mean response in MSLP and surface temperature averaged over the months following events in which U (60°N, 10 hPa) is less than two standard deviations below its mean value (i.e., an anomalously weak polar vortex), for both the high and low top models. An anomalously negative NAM, as seen in Fig. 12d, is now apparent in both models, along with the associated response in surface temperature. The pattern of the response in the high top model more closely matches the observations than that in the low top model, which differs substantially over parts of the Atlantic and North America.

As mentioned above, a transition to easterly winds, as occurs during an SSW, will also prevent planetary wave propagation into the stratosphere. A realistic simulation of easterly winds in the Northern Hemisphere winter stratosphere, and a realistic number of SSWs, is found here to require a high top model.

6. Conclusions

Using the high top simulations run with the Met Office Unified Model for CMIP5, and equivalent low top

simulations, the influence of including a well-resolved stratosphere in general circulation model climate simulations on surface climate has been considered. The historical period 1960–2002 was analyzed, and compared against the ERA-40 reanalysis.

Surface temperature is well simulated in the high and low top models, with only a 1-K cold bias in the global mean temperature, and with the highest interannual variability in temperature being found in the El Niño and extratropical regions in both the reanalysis and the models. However, there is a 3-K cold bias in the northern extratropics, which is slightly greater in the high top model, and a 1.6-K warm bias over the Southern Ocean thought to be due to biases in cloud cover and ocean heat transport. These biases lead to around 1×10^6 km^2 too much Arctic sea ice in the high top model, and around 2.5×10^6 km^2 too little Antarctic sea ice in both models.

Much of the extratropical variability found in surface temperature projects onto the annular modes. By considering the observed and simulated distributions of 30-yr North Atlantic Oscillation (NAO) index trends from 1860–2000 it is found that the NAO trends as simulated by the models are not inconsistent with those in the observations. The observed 12 hPa $(30\ \text{yr})^{-1}$ trend in the NAO index from 1965 to 1995 is the largest 30-yr trend seen in at least the last 140 years. That the models do not capture as large a trend over the same 30 years is perhaps to be expected since the NAO has been linked to internal decadal variability in the stratospheric zonal mean zonal wind and the ocean circulation. On the other hand, Joshi et al. (2006) suggest that changes in stratospheric water vapor may influence the NAO and may have contributed to the increasing NAO index observed from 1965 to 1995, and it may be that the models do not capture this process.

The observed increase in the southern annular mode (SAM) index from 1960 to 2000 is believed to be forced, in part, by stratospheric ozone depletion, though again the distinction between ''forced'' and ''internal'' variability of this mode is not obvious. A cooling of the polar lower stratosphere and consequent increase with altitude in zonal mean zonal wind in the extratropical lower stratosphere is simulated by both high and low top models. However, this cooling is weaker than that observed and thus the trend in zonal mean zonal wind is weaker than that observed. This weaker signal is not communicated to the surface, and the tropospheric trend in the zonal wind, and tropospheric temperature gradient, is found to be the same in the historical simulations as it is in simulations run with constant 1960s ozone concentrations (which lack the lower-stratospheric cooling seen in the historical runs).

Both high and low top models used in this study simulate realistic basic climate and interannual variability. Little distinction is found between the high and low top model simulations, until the effects of teleconnections on surface fields during specific years is considered. One such teleconnection is that of the El Niño–Southern Oscillation (ENSO) on northern extratropical mean sea level pressure (MSLP). The signal of anomalously high MSLP at the pole and anomalously low MSLP in the extratropics in ENSO years is captured with greater amplitude by the high top model than by the low top model. The stratospheric pathway for this teleconnection is via a weakening of the stratospheric polar vortex in ENSO years, a signal found to be stronger in the high top model than in the low top model.

A direct influence of the quasi-biennial oscillation (QBO) of tropical stratospheric winds on surface zonal wind and MSLP, and of midwinter stratospheric sudden warmings of the polar vortex on extratropical MSLP and temperature is found in the high top model. The low top model, which does not simulate the QBO and simulates very few stratospheric sudden warmings (reversal of the zonal mean wind in the middle stratosphere), will be for the most part unable to simulate these influences on surface climate. The low top model does simulate realistic polar vortex variability, however, and thus the influence this has on MSLP is captured by both models.

The ability to simulate such processes as ENSO teleconnections and stratospheric sudden warmings potentially aids predictability of surface climate on a seasonal to decadal time scale, although not beyond the predictability of the processes themselves (around a year for ENSO and a few weeks for stratospheric sudden warmings). It is therefore suggested that, in order to capture the important influence of teleconnections and stratospheric processes on surface climate shown here, climate simulations should be performed using stratosphere-resolving general circulation models.

Acknowledgments. The authors thank Dr. Adam Scaife for useful discussions about the North Atlantic Oscillation and stratospheric sudden warmings, and Dr. Bill Collins and three anonymous reviewers for general comments on this work. The work of SCH and NB was supported by the Joint DECC/Defra Met Office Hadley Centre Climate Programme (GA01101) and also by the European Commission's Seventh Framework Programme, under Grant Agreement 226520, COMBINE Project. ERA-40 data used in this study have been obtained from the ECMWF data server.

REFERENCES

Allan, R., and T. Ansell, 2006: A new globally complete monthly historical gridded mean sea level pressure dataset (HadSLP2): 1850–2004. *J. Climate,* **19,** 5816–5842.

Arblaster, J. M., and G. A. Meehl, 2006: Contributions of external forcings to southern annular mode trends. *J. Climate,* **19,** 2896–2905.

Baldwin, M. P., and T. J. Dunkerton, 1999: Propagation of the Arctic Oscillation from the stratosphere to the troposphere. *J. Geophys. Res.,* **104** (D24), 30 937–30 946.

Bell, C. J., L. J. Gray, A. J. Charlton-Perez, M. M. Joshi, and A. A. Scaife, 2009: Stratospheric communication of El Niño teleconnections to European winter. *J. Climate,* **22,** 4083–4096.

Braesicke, P., and J. A. Pyle, 2004: Sensitivity of dynamics and ozone to different representations of SSTs in the Unified Model. *Quart. J. Roy. Meteor. Soc.,* **130,** 2033–2045, doi:10.1256/qj.03.183.

Bushell, A. C., D. R. Jackson, N. Butchart, S. C. Hardiman, T. J. Hinton, S. M. Osprey, and L. J. Gray, 2010: Sensitivity of GCM tropical middle atmosphere variability and climate to ozone and parameterized gravity wave changes. *J. Geophys. Res.,* **115,** D15101, doi:10.1029/2009JD013340.

Butchart, N., J. Austin, J. R. Knight, A. A. Scaife, and M. L. Gallani, 2000: The response of the stratospheric climate to projected changes in the concentrations of well-mixed greenhouse gases from 1992 to 2051. *J. Climate,* **13,** 2142–2159.

Cagnazzo, C., and E. Manzini, 2009: Impact of the stratosphere on the winter tropospheric teleconnections between ENSO and the North Atlantic and European region. *J. Climate,* **22,** 1223–1238.

Charlton, A. J., and L. M. Polvani, 2007: A new look at stratospheric sudden warmings. Part I: Climatology and modeling benchmarks. *J. Climate,* **20,** 449–469.

Garfinkel, C. I., and D. L. Hartmann, 2011: The influence of the quasi-biennial oscillation on the troposphere in winter in a hierarchy of models. Part I: Simplified dry GCMs. *J. Atmos. Sci.,* **68,** 1273–1289.

Hardiman, S. C., N. Butchart, S. M. Osprey, L. J. Gray, A. C. Bushell, and T. J. Hinton, 2010: The climatology of the middle atmosphere in a vertically extended version of the Met Office's climate model. Part I: Mean state. *J. Atmos. Sci.,* **67,** 1509–1525.

Hoerling, M. P., J. W. Hurrell, T. Xu, G. T. Bates, and A. Phillips, 2004: Twentieth century North Atlantic climate change. Part II: Understanding the effect of Indian Ocean warming. *Climate Dyn.,* **23** (3–4), 391–405, doi:10.1007/s00382-004-0433-x.

Huebener, H., U. Cubasch, U. Langematz, T. Spangehl, F. Niehörster, I. Fast, and M. Kunze, 2007: Ensemble climate simulations using a fully coupled ocean–troposphere–stratosphere general circulation model. *Philos. Trans. Roy. Soc. London,* **365A** (1857), 2089–2101, doi:10.1098/rsta.2007.2078.

Ineson, S., and A. A. Scaife, 2009: The role of the stratosphere in the European climate response to El Niño. *Nat. Geosci.,* **2,** 32–36, doi:10.1038/ngeo381.

Jones, C. D., and Coauthors, 2011: The HadGEM2-ES implementation of CMIP5 centennial simulations. *Geosci. Model Dev.,* **4,** 543–570, doi:10.5194/gmd-4-543-2011.

Joshi, M. M., A. J. Charlton, and A. A. Scaife, 2006: On the influence of stratospheric water vapor changes on the tropospheric circulation. *Geophys. Res. Lett.,* **33,** L09806, doi:10.1029/2006GL025983.

Kolstad, E. W., T. Breiteig, and A. A. Scaife, 2010: The association between stratospheric weak polar vortex events and cold air outbreaks. *Quart. J. Roy. Meteor. Soc.,* **136,** 886–893.

Lenton, A., F. Codron, L. Bopp, N. Metzl, P. Cadule, A. Tagliabue, and J. Le Sommer, 2009: Stratospheric ozone depletion reduces ocean carbon uptake and enhances ocean acidification. *Geophys. Res. Lett.,* **36,** L12606, doi:10.1029/2009GL038227.

Le Quéré, C., and Coauthors, 2007: Saturation of the Southern Ocean CO_2 sink due to recent climate change. *Science,* **316** (5832), 1735–1738, doi:10.1126/science.1136188.

Mantua, N. J., and S. R. Hare, 2002: The Pacific Decadal Oscillation. *J. Oceanogr.,* **58** (1), 35–44, doi:10.1023/A:1015820616384.

Manzini, E., M. A. Giorgetta, M. Esch, L. Kornblueh, and E. Roeckner, 2006: The influence of sea surface temperatures on the northern winter stratosphere: Ensemble simulations with the MAECHAM5 model. *J. Climate,* **19,** 3863–3881.

Marshall, A. G., and A. A. Scaife, 2009: Impact of the QBO on surface winter climate. *J. Geophys. Res.,* **114,** D18110, doi:10.1029/2009JD011737.

——, and ——, 2010: Improved predictability of stratospheric sudden warming events in an AGCM with enhanced stratospheric resolution. *J. Geophys. Res.,* **115,** D16114, doi:10.1029/2009JD012643.

Martin, G. M., and Coauthors, 2011: The HadGEM2 family of Met Office Unified Model climate configurations. *Geosci. Model Dev.,* **4,** 723–757, doi:10.5194/gmd-4-723-2011.

Osborn, T. J., and P. D. Jones, 2000: Air flow influences on local climate: Observed United Kingdom climate variations. *Atmos. Sci. Lett.,* **1,** 62–74, doi:10.1006/asle.2000.0013.

Osprey, S. M., L. J. Gray, S. C. Hardiman, N. Butchart, A. C. Bushell, and T. J. Hinton, 2010: The climatology of the middle atmosphere in a vertically extended version of the Met Office's Climate Model. Part II: Variability. *J. Atmos. Sci.,* **67,** 3637–3651.

Park, W., and M. Latif, 2008: Multidecadal and multicentennial variability of the meridional overturning circulation. *Geophys. Res. Lett.,* **35,** L22703, doi:10.1029/2008GL035779.

Perlwitz, J., and N. Harnik, 2004: Downward coupling between the stratosphere and troposphere: The relative roles of wave and zonal mean processes. *J. Climate,* **17,** 4902–4909.

Rayner, N. A., D. E. Parker, E. B. Horton, C. K. Folland, L. V. Alexander, D. P. Rowell, E. C. Kent, and A. Kaplan, 2003: Global analyses of sea surface temperature, sea ice, and night marine air temperature since the late nineteenth century. *J. Geophys. Res.,* **108,** 4407, doi:10.1029/2002JD002670.

Sassi, F., R. R. Garcia, D. Marsh, and K. W. Hoppel, 2010: The role of the middle atmosphere in simulations of the troposphere during Northern Hemisphere winter: Differences between high- and low-top models. *J. Atmos. Sci.,* **67,** 3048–3064.

Scaife, A. A., and J. R. Knight, 2008: Ensemble simulations of the cold European winter of 2005–2006. *Quart. J. Roy. Meteor. Soc.,* **134,** 1647–1659, doi:10.1002/qj.312.

——, N. Butchart, C. D. Warner, D. Stainforth, W. Norton, and J. Austin, 2000: Realistic Quasi-Biennial Oscillations in a simulation of the global climate. *Geophys. Res. Lett.,* **27** (21), 3481–3484.

——, ——, ——, and R. Swinbank, 2002: Impact of a spectral gravity wave parametrization on the stratosphere in the Met Office Unified Model. *J. Atmos. Sci.,* **59,** 1473–1489.

——, J. R. Knight, G. K. Vallis, and C. K. Folland, 2005: A stratospheric influence on the winter NAO and North Atlantic surface climate. *Geophys. Res. Lett.,* **32,** L18715, doi:10.1029/2005GL023226.

Schneider, N., and B. D. Cornuelle, 2005: The forcing of the Pacific decadal oscillation. *J. Climate,* **18,** 4355–4373.

Shaw, T. A., and J. Perlwitz, 2010: The impact of stratospheric model configuration on planetary-scale waves in Northern Hemisphere winter. *J. Climate,* **23,** 3369–3389.

Sigmond, M., J. F. Scinocca, and P. J. Kushner, 2008: Impact of the stratosphere on tropospheric climate change. *Geophys. Res. Lett.,* **35,** L12706, doi:10.1029/2008GL033573.

Simmons, A. J., A. Untch, C. Jakob, P. Kållberg, and P. Undén, 1999: Stratospheric water vapour and tropical tropopause temperatures in ECMWF analyses and multi-year simulations. *Quart. J. Roy. Meteor. Soc.,* **125** (553), 353–386, doi:10.1002/qj.49712555318.

Solomon, S., D. Qin, M. Manning, M. Marquis, K. Averyt, M. M. B. Tignor, H. L. Miller Jr., and Z. Chen, Eds., 2007: *Climate Change 2007: The Physical Science Basis*. Cambridge University Press, 996 pp.

Son, S. W., and Coauthors, 2010: Impact of stratospheric ozone on Southern Hemisphere circulation change: A multimodel assessment. *J. Geophys. Res.,* **115,** D00M07, doi:10.1029/2010JD014271.

Thompson, D. W. J., and S. Solomon, 2002: Interpretation of recent Southern Hemisphere climate change. *Science,* **296** (5569), 895–899, doi:10.1126/science.1069270.

Untch, A., and A. J. Simmons, 1999: Increased stratospheric resolution in the ECMWF forecasting system. *ECMWF Newsletter*, No. 82, European Centre for Medium-Range Weather Forecasts, Reading, United Kingdom, 2–8.

Uppala, S. M., and Coauthors, 2005: The ERA-40 Re-Analysis. *Quart. J. Roy. Meteor. Soc.,* **131,** 2961–3012, doi:10.1256/qj.04.176.

van Loon, H., and R. A. Madden, 1981: The Southern Oscillation. Part I: Global associations with pressure and temperature in northern winter. *Mon. Wea. Rev.,* **109,** 1150–1162.

Wallace, J. M., 2000: North Atlantic Oscillation/annular mode: Two paradigms—one phenomenon. *Quart. J. Roy. Meteor. Soc.,* **126** (564), 791–805.

Warner, C. D., and M. E. McIntyre, 1999: Toward an ultra-simple spectral gravity wave parameterization for general circulation models. *Earth Planets Space,* **51,** 475–484.